A sodium-ion battery exploiting layered oxide cathode, graphite anode and glyme-based electrolyte

Ivana Hasa[a,b,c], Xinwei Dou[b,c], Daniel Buchholz[b,c], Yang Shao-Horn[d,e,f], Jusef Hassoun[a,g]* Stefano Passerini[b,c]* and Bruno Scrosati[b,h]*

[a] Department of Chemistry, "Sapienza" University of Rome, Piazzale Aldo Moro, 5, 00185 Rome, Italy.

[b] Helmholtz Institute Ulm, Helmholtzstraße 11, 89081 Ulm, Germany.

[c] Karlsruhe Institute of Technology (KIT), PO Box 3640, 76021 Karlsruhe, Germany.

[d] Electrochemical Energy Laboratory, Massachusetts Institute of Technology, Cambridge, Massachusetts 02139, USA.

[e]Department of Mechanical Engineering, Massachusetts Institute of Technology, Cambridge, Massachusetts 02139, USA.

[f] Department of Materials Science and Engineering, Massachusetts Institute of Technology, Cambridge, Massachusetts 02139, USA.

[g] Italian Institute of Technology, Via Morego 30, 16163 Genova, Italy.

[h] Department of Chemical and Pharmaceutical Sciences, University of Ferrara, Via Fossato di Mortara, 44121, Ferrara, Italy

*jusef.hassoun@unife.it, stefano.passerini@kit.edu, bruno.scrosati@gmail.com

Keywords

Sodium-ion battery, graphite anode, layered oxide cathode, glyme based electrolyte, high-power.

Abstract

Room-temperature rechargeable sodium-ion batteries (SIBs), in view of the large availability and low cost of sodium raw materials, represent an important class of electrochemical systems suitable for application in large-scale energy storage. In this work, we report a novel, high power SIB formed by coupling the layered P2-$Na_{0.7}CoO_2$ cathode with the graphite anode in an optimized ether-based electrolyte. The study firstly addresses the electrochemical optimization of the two electrode materials and then the realization and characterization of the novel SIB based on their combination. The cell represents an original *sodium rocking chair battery* obtained combining the intercalation/de-intercalation processes of sodium within the cathode and anode layers. We show herein that this battery, favored by suitable electrode/electrolyte combination, offers unique performance in terms of cycle life, efficiency and, especially, power capability.

1. Introduction

The great employment of non-renewable fossil fuels, presently one of the mayor responsible for greenhouse gas emission and atmosphere pollution, has driven the interest on alternative energy plants and more environmentally friendly power sources [1,2]. The large attention devoted to the development of renewable energy sources and new technologies for energy conversion and storage have led to the achievement of high performance and efficient rechargeable electrochemical systems [3,4]. Batteries based on the use of alkali metals, such as lithium and sodium have been identified as the most suitable since 1980s. However, the great success of lithium-ion batteries so far mitigated the interest on SIB technology [5]. Recent concerns on long-term availability, limited geographical localization and increasing price of lithium, triggered renewed interest on alternative rechargeable batteries [6–8]. Sodium-ion batteries (SIBs) represent the most interesting alternative to lithium due to high abundance, low cost and large availability of the sodium precursors [9,10]. A relevant number of suitable materials

have been identified [11–13], including cathodes, anodes as well as electrolytes, however only few prototypes of full SIBs have been reported [14–19].

In fact, the golden electrode combination ($LiCoO_2$-graphite) identified for lithium-ion batteries more than two decades ago, has not been identified for SIBs, yet. However, both $Na_{0.7}CoO_2$ [20] and graphite [21] have revealed surprising differences in half and full cells in respect to the analogues lithium-based materials. Sodium cobalt oxide revealed poor performances in terms of cycling stability and efficiency of the Na (de-)insertion process [22–27]. These issues have been attributed to inappropriate selection of the electrolyte solution. Indeed, $NaPF_6$-EC:PC proposed by Ponrouch *et al* [28] as standard electrolyte for sodium-ion batteries led to poor stability, while $NaClO_4$-EC:DMC solution reported by J.J. Ding *et al* [26] evidenced improved cycle life, however, low Coulombic efficiency. This issue might be mitigated in principle, by the addition of fluoroethylene carbonate (FEC) to the electrolyte solution [15]. Furthermore, several successes have been achieved by partially substituting cobalt with different metals, such as Fe, Ni and Mn within the layered structure [29–33].

Among the anodes, sodium conversion [34,35] and alloying [16,36,37] compounds, as well as hard and soft carbons [38] appeared the most suitable for application in SIB. Recently, expanded graphite has been proposed as anode with very promising cycling behavior in terms of capacity retention, however showing limited rate capability [39]. In contrast, the use of graphite, i.e., the most widely diffused anode for LIB, has been so far hindered in SIB by the unfavorable graphitic interlayer distance compared to the ionic radio of sodium ions. Recent study in diglyme-based electrolyte demonstrated that the co-intercalation phenomena of ternary GICs (graphite intercalation compounds), i.e., solvated sodium ions, enables the sodium storage within the graphite, thus allowing its use as anode for SIBs [21].

Herein, we originally disclose an enhanced, high-power SIB based on a layered oxide cathode and a graphite anode. We show that this battery, exploiting the combination of an intercalation chemistry

at the cathode side and a co-intercalation phenomenon at the anode side, has unique electrochemical properties that make it suitable for stationary energy storage applications.

2. Experimental

2.1 Material synthesis and characterization

P2- type layered $Na_{0.7}CoO_2$ was synthesized by solid-state reaction. The precursors (Sigma Aldrich) were used as received without further purification. Anhydrous sodium carbonate (Na_2CO_3, ACS reagent, ≥99.5%) and cobalt oxide (Co_3O_4, Co(II,III) oxide powder) were pre-dried respectively at 120 °C and 400 °C for 2 hours. Following, the powders were mixed and grinded. After the achievement of an homogeneous mixture, the pelletized material was subjected to a thermal treatment at 850 °C for 15 hours in air atmosphere and finally quenched to room temperature. In order to compensate the sodium loss at high temperature, an excess of 10% of Na_2CO_3 in respect to the desired amount has been used. The elemental composition, obtained by inductively coupled plasma optical emission spectrometry (ARCOS ICP-OES, Spectro Analytical Instruments, Kleve, Germany), was determined from the Na/Co ratio, assuming no oxygen deficiencies. The structural and morphological characterization of the sample were investigated by X-Ray Diffraction (XRD, Rigaku Dmax Ultima + X-ray diffractometer) with CuK_α radiation, in the 2θ range from 10° to 90°, and by scanning electron microscopy using a Phenom-FEI instrument, respectively. Natural graphite (SLP-30, IMERYS) was used as received without any further treatment. The electrolytes were prepared in an argon-filled dry box with an oxygen and water content lower than 1 ppm. Before use, solvents have been dried by using 4Å zeolite type for several days, until a water content lower than 10 ppm as detected by Karl Fisher titration. $NaClO_4$ (sodium perchlorate) salt was dried under vacuum overnight at 180°C and dissolvent in various solvents in a 1 mol L^{-1} ratio. The solvents used for electrolyte preparation were EC:DMC (1:1 w/w) (ethylene carbonate:dimethyl

carbonate), EC:DMC(1:1 w/w)+20%weight FEC (fluoroethylene carbonate) and TEGDME (tetraethylene glycol dimethyl ether).

2.2 Electrochemical characterization

The electrochemical tests were run using Swagelok-type cells assembled in an argon-filled glove box. Sodium half-cells were assembled by using glass fiber (Whatman) as separators soaked in various electrolyte solutions and sodium metal as counter and reference electrode. Sodium metal was cut from sodium pieces (99.8%, Acros Organics), roll pressed and punched on the current collector. The $Na_{0.7}CoO_2$ electrodes were prepared by doctor-blade casting on Al of a slurry prepared by dispersing 80 wt% of active material, 10 wt% of carbon black conductive agent (Super C65, IMERYS) and 10 wt% of polyvinylidenefluoride (PVDF 6020 Solef, Arkema Group) binder in N-methyl-2-pyrrolidone (NMP). Graphite electrodes were prepared by casting on Cu foil a slurry composed by active material, Super C65 carbon conductor (IMERYS) and Carboxymethyl cellulose (CMC, Walocel 2000PA, 1.2 substitution degree) binder in an 85:5:10 weight ratio. Following, electrodes of 12-mm diameter, loaded by 2 mg of $Na_{0.7}CoO_2$ and 6 mg of graphite, respectively, have been punched, pressed and dried. The cells were assembled in an argon-filled glove box with H_2O and O_2 content lower than 1 ppm. A Maccor 4000 Battery system was used for the galvanostatic cycling tests. The cells were cycled at various current rates, within the 0.02V to 2.0V vs Na^+/Na for graphite half-cells, 3.8V-2.0V vs Na^+/Na for $Na_{0.7}CoO_2$ half-cells and 3.7V-0.5V for Graphite/$Na_{0.7}CoO_2$ full-cells. Prior full-cells assembly, graphite anodes were electrochemically activated by pre-cycling in order to remove the irreversible capacity exhibited during the first discharge and to provide a sodium source able to compensate the sodium deficiency of the P2-type cathode.

3. Results and discussion

3.1 The P2-$Na_{0.7}CoO_2$ electrode

The structural and morphological characterization of $Na_{0.7}CoO_2$ are shown in Fig. 1. The XRD pattern (Fig. 1a) matches with the typical P2-type layered structure reported for the γ-$Na_{0.71}Co_{0.96}O_2$ phase (JCPD # 00-030-1182). The P2-$Na_{0.7}CoO_2$ crystallizes in the hexagonal $P6_3/mmc$ space group, displaying an ABBA arrangements of $(CoO_2)_n$ sheets formed by CoO_6 edge-sharing octahedral units among which Na^+ ions can be hosted in two different types of trigonal prismatic sites, sharing faces (Na_f) with two CoO_6 octahedra belonging to adjacent layers or edges (Na_e) with six CoO_6 surrounding octahedral units [20,22]. The SEM micrographs (Fig. 1b) reveal that $Na_{0.7}CoO_2$ particles are formed by adherent planes of hexagonal symmetry, with size ranging from 5 to 10 μm, thus reflecting the layered morphology of the cathode material.

Figure 1

The electrochemical characterization of the $Na_{0.7}CoO_2$ cathode (Fig. 2) is performed in sodium half-cell using two versions of a common EC:DMC-$NaClO_4$ electrolyte, i.e. a bare version and an upgraded solution added by FEC [15]. The first charge-discharge profile in the bare solution (inset of Fig. 2a) exhibits a first de-sodiation process characterized by four plateaus and a capacity of about 80 mAh g^{-1}, while the following sodiation process, delivering about 84 mAh g^{-1}, evolves through eight plateaus corresponding to the various phase transitions already described by Berthelot *et al* [20]. Subsequently, the charge-discharge process of the sodium cell reversibly proceeds following the above eight voltage plateaus, centered at about 3V vs. Na^+/Na (Fig. 2a). Despite a lower capacity of $Na_{0.7}CoO_2$ during the first discharge in the FEC-added electrolyte (65 mAh g^{-1}, Fig. 2b), the reversible capacity of the cell remarkably increases up to about 105 mAh g^{-1} during the following cycles. The lower capacity during first charge in the upgraded electrolyte, already observed in a previous work [15], may be most

likely attributed to the formation of a passivation layer at the cathode surface partially hindering the de-sodiation process. The cathode passive layer is modified during the following cycles, thus efficiently allowing the electrochemical process [40,41]. Indeed, the comparison of the cycling trend (Fig. 2c) clearly shows the expected increase of both coulombic efficiency (from 95% to about 100%) and capacity (from 80 to 100 mAh g^{-1}) by FEC addition.

Figure 2

Taking into account the results reported in Fig.2, the rate capability of the $Na_{0.7}CoO_2$ cathode is investigated in the EC:DMC-$NaClO_4$-FEC electrolyte (Fig. 3). The electrode delivers capacity of about 100 mAh g^{-1} at 0.2C, 80 mAh g^{-1} at 1C and still a residual capacity of about 70 mAh g^{-1} when cycled at the very high rate of 10C, following the expected voltage signature with low polarization (Fig. 3a), stable trend and efficiency exceeding 99% (Fig. 3b). This remarkable performance is attributed to the high diffusion coefficient of sodium ions in layered cobalt oxides ($D \sim 0.5\text{-}1.5\times10^{-10}$ cm^2 s^{-1},which is a value even higher than those of Li^+ in $LiCoO_2$) and to the high electronic conductivity of cobalt (metallic conduction $\sigma \approx 300$ S cm^{-1}), which greatly improves the kinetic of the sodium (de)-insertion reaction into the host structure [42,43]. The cell can recover about 98% of the initial capacity by decreasing the current from 10C back to 0.2C, thus further accounting for the structural stability of the $Na_{0.7}CoO_2$ electrode. Moreover, even after the stressful rate capability test, the material exhibits a capacity retention of about 92% after 100 cycles with an efficiency approaching 100% (Fig.3b).

Figure 3

3.2 The Graphite electrode

A first attempt for graphite anode characterization in sodium half-cell is conducted by employing the two electrolytes above described, i.e., bare EC:DMC-$NaClO_4$ and FEC-added one (Fig. 4a, green and black curves, respectively). However, both the carbonate-based electrolytes revealed a very poor

behavior, with very limited signs of sodium intercalation process in the sodium cell. The poor electrochemical performance may be ascribed to the unfavorable graphitic interlayer distance compared to the ionic radio of sodium ions in carbonate-based electrolyte media that hinders the formation of binary GICs, which should enable the Na-intercalation process [21,44]. In contrast, the use of glyme-based electrolyte, i.e. 1M TEGDME-$NaClO_4$, enables the co-intercalation of solvated sodium ions by forming ternary GICs (graphite intercalation compounds) [44] following an electrochemical process centered at about 0.77V vs. Na^+/Na (Fig. 4a, red curve). It has been demonstrated that the voltage plateau for Na storage increases according to the chain length of the glyme-based solvent, suggesting that higher potential values for Na storage indicate more stable discharge products [44].

This process allows reversible cell operation for 500 cycles at 1C, with a capacity of about 100 mAh g^{-1}, a steady state efficiency approaching 100% and a retention as high as 99 % (Fig. 4b). The rate capability test of the graphite anode in sodium cell using the glyme-based electrolyte (Fig. 4c) shows, after an activation cycle performed at 0.1C, a capacity ranging from 100 mAh g^{-1} at 0.2C to about 90 mAh g^{-1} at current rate as high as 10C. The cell completely recovers its initial capacity when the current is lowered back to 1C. The voltage profile during the test reported in Fig. 4d evidences relevant capacity retention and almost no effect of the increasing current on the polarization, thus further accounting for the high rate capability of the cell.

Figure 4

Considering the excellent capacity retention and the high rate capability of both cathode and anode, we expect that their combination may lead to a full SIB characterized by long cycle life and high power. However, prior to combining anode and cathode, the high performance of the P2-$Na_{0.7}CoO_2$ should be confirmed in the TEGDME-based solution, that is, the most suitable electrolyte for the anode. Accordingly, Fig. S1 and related discussion in the Supplementary Information (SI) section confirm that, despite a lower rate capability in particular at the very high currents in respect to carbonate solution, the

$Na_{0.7}CoO_2$ electrode efficiently operates in the TEGDME-based electrolyte. Moreover, the additional electrochemical tests on sodium half-cells using a $Na_{0.7}CoO_2$ electrode and electrolytes containing different salts, well supported the choice of $NaClO_4$ as sodium salt rather than others such as $NaCF_3SO_3$ and $NaPF_6$ (see Fig. S2 in the Supplementary Information).

3.3 The full sodium-ion cell

Prior to assembly the full-cell, the graphite anode has been electrochemically activated in sodium half-cells in order to remove its small irreversible capacity and achieve a partial sodium intercalation for compensation of the sodium deficiency of the cathode used without pre-cycling [15]. Figure 5a reports the voltage profiles of the Graphite/TEGDME-$NaClO_4$/ $Na_{0.7}CoO_2$ full SIB cycled within the 3.7–0.5 V voltage range at 1C (175 mA g^{-1}). The first cycle reveals the expected lower charge capacity in respect to the discharge ascribed to the above discussed sodium deficiency in the cathode that is used without any activation (compare with Fig. S1b in SI section). At the steady state, the cell operates with an average voltage value of about 2.2V with a profile reflecting the combination of sodium (-de) intercalation within cathode and anode layers following a *sodium rocking chair* process and delivering a reversible capacity of about 80 mAh g^{-1}, upon 100 cycles. The rate capability of the SIB is investigated from 1C to 10C (i.e., from 175 to 1750 mA g^{-1}) both in terms of voltage profile (Fig. 5b) and cycling trend (Fig. 5c). The results show a voltage slightly affected by the increasing current from 1C to 2C and well reflecting the efficient electrochemical process (compare Fig. 5b and Fig. 3a), while the very high currents (5C and 10C) lead to an increase of the polarization, as indeed expected by the rising ohmic drop of the cell. The cycling curves (Fig. 5c) show a delivered capacity ranging from about 80 mAh g^{-1} at 1C to 60 mAh g^{-1} at 5C and to 40 mAh g^{-1} at 10C with efficiency always approaching 100% at the steady state. Moreover, the high-rate cycling test at 10C prolonged to more than 1200 cycles (Fig. 5d) reveals a capacity retention as high as 80%, i.e., a value well suitable for battery application. Despite the low energy density, expected

to practically range from about 60 Wh kg^{-1} at 1C to 30 Wh kg^{-1} at 10C basing on the cell capacity and its average working voltage, the remarkable rate capability and cycle life represent a very appealing characteristics for high-power applications [45]. Indeed, our cell configuration allows at 10C the achievement of about 45% of its maximum capacity that corresponds to 6 minutes of charge or discharge, extended for more than 1000 cycles.

Figure 5

4. Conclusions

We report in this work, a novel type of sodium ion battery exploiting a layered P2-type $Na_{0.7}CoO_2$ cathode combined with a graphite anode in an optimized, glyme-based electrolyte. As typical for SIBs, also the one here presented has a lower energy density than LIBs, however it offers unique characteristics of long cycle life, high efficiency and, especially, high power density which make the cell quite attracting for large-scale energy storage application. We have shown here that our SIB is able to operate at a rate as high as 10C, which makes it able to complete a full cycle in 12 minutes, thus meeting the duration required by energy storage systems, such as frequency regulation, peak reduction and demand shifting, where the typical cycling operation ranges from 1 to 40 per day. In addition, we report in this work the development and characterization of a cathode material having unique rate capability, as well as we confirm of the applicability of plain graphite as anode in sodium cells, when combined with a proper electrolyte. Certainly, we are aware that our SIB still requires optimization, especially in terms of overall cell balancing so as to properly address the initial irreversible capacity and finally increase its overall electrochemical behavior. On the other hand, the above-mentioned characteristics of long life and, especially of high power, encouraged us to believe that report this work, even if still in a preliminary stage, might be of concrete interest for the battery community.

Acknowledgments

BS is very grateful to the Karlsruhe Institute of Technology for a Visiting Professor Fellowship. XD, DB and SP wish to thank the financial support of the European Commission within the FP7-ENERGY-2013-1 Project INFLUENCE (Grant number: 608621). IMERYS and ARKEMA are acknowledged for kindly providing SLP30 and Super C65, and PVDF, respectively.

References

[1] D. Larcher, J. Tarascon, Nat. Chem. 7 (2015) 19–29.

[2] I. Hadjipaschalis, A. Poullikkas, V. Efthimiou, Renew. Sustain. Energy Rev. 13 (2009) 1513–1522.

[3] P.J. Hall, E.J. Bain, Energy Policy. 36 (2008) 4352–4355.

[4] H.D. Yoo, E. Markevich, G. Salitra, D. Sharon, D. Aurbach, Mater. Today. 17 (2014) 110–121.

[5] N.S. Choi, Z. Chen, S. a. Freunberger, X. Ji, Y.K. Sun, K. Amine, et al., Angew. Chemie - Int. Ed. 51 (2012) 9994–10024.

[6] F. Risacher, B. Fritz, Aquat. Geochemistry. 15 (2009) 123–157.

[7] A. Yaksic, J.E. Tilton, Resour. Policy. 34 (2009) 185–194.

[8] J.-M. Tarascon, Nat. Chem. 2 (2010) 510–510.

[9] B.L. Ellis, L.F. Nazar, Curr. Opin. Solid State Mater. Sci. 16 (2012) 168–177.

[10] H. Pan, Y.-S. Hu, L. Chen, Energy Environ. Sci. 6 (2013) 2338–2360.

[11] N. Yabuuchi, K. Kubota, M. Dahbi, S. Komaba, Chem. Rev. 114 (2014) 11636–11682.

[12] S.W. Kim, D.H. Seo, X. Ma, G. Ceder, K. Kang, Adv. Energy Mater. 2 (2012) 710–721.

[13] M. Sawicki, L.L. Shaw, RSC Adv. 5 (2015) 53129–53154.

[14] I. Hasa, J. Hassoun, Y.K. Sun, B. Scrosati, ChemPhysChem. 15 (2014) 2152–2155.

[15] I. Hasa, S. Passerini, J. Hassoun, RSC Adv. 5 (2015) 48928–48934.

[16] D.-J. Lee, J.-W. Park, I. Hasa, Y.-K. Sun, B. Scrosati, J. Hassoun, J. Mater. Chem. A. 1 (2013) 5256–5261.

[17] D. Kim, E. Lee, M. Slater, W. Lu, S. Rood, C.S. Johnson, Electrochem. Commun. 18 (2012) 66–69.

[18] A. Ponrouch, R. Dedryvere, D. Monti, A.E. Demet, J.M. Ateba Mba, L. Croguennec, et al., Energy Environ. Sci. 6 (2013) 2361–2369.

[19] S. Komaba, W. Murata, T. Ishikawa, N. Yabuuchi, T. Ozeki, T. Nakayama, et al., Adv. Funct. Mater. 21 (2011) 3859–3867.

[20] R. Berthelot, D. Carlier, C. Delmas, Nat. Mater. 10 (2011) 74–80.

[21] B. Jache, P. Adelhelm, Angew. Chemie - Int. Ed. 53 (2014) 10169–10173.

[22] C. Delmas, C. Fouassier, P. Hagenmuller, Phys. B+C. 99 (1980) 81–85.

[23] C. Fouassier, G. Matejka, J.-M. Reau, P. Hagenmuller, J. Solid State Chem. 6 (1973) 532–537.

[24] L.W. Shacklette, T.R. Jow, L. Towsend, J. Electrochem. Soc. 135 (1988) 2669–2674.

[25] A. Bhide, J. Hofmann, A.K. Dürr, J. Janek, P. Adelhelm, Phys. Chem. Chem. Phys. 16 (2014) 1987–1998.

[26] J.J. Ding, Y.N. Zhou, Q. Sun, X.Q. Yu, X.Q. Yang, Z.W. Fu, Electrochim. Acta. 87 (2013) 388–393.

[27] M. D'Arienzo, R. Ruffo, R. Scotti, F. Morazzoni, C.M. Mari, S. Polizzi, Phys. Chem. Chem. Phys. 14 (2012) 5945–5952.

[28] A. Ponrouch, E. Marchante, M. Courty, J.-M. Tarascon, M.R. Palacín, Energy Environ. Sci. 5 (2012) 8572–8583.

[29] I. Hasa, D. Buchholz, S. Passerini, B. Scrosati, J. Hassoun, Adv. Energy Mater. (2014). doi:10.1002/aenm.201400083.

[30] I. Hasa, D. Buchholz, S. Passerini, J. Hassoun, ACS Appl. Mater. Interfaces. 7 (2015) 5206–5212.

[31] D. Yuan, X. Hu, J. Qian, F. Pei, F. Wu, R. Mao, et al., Electrochim. Acta. 116 (2014) 300–305.

[32] N. Yabuuchi, M. Kajiyama, J. Iwatate, H. Nishikawa, S. Hitomi, R. Okuyama, et al., Nat. Mater. 11 (2012) 512–517.

[33] J. Billaud, J. Cle, A.R. Armstrong, P. Rozier, C.P. Grey, P.G. Bruce, J. Am. Chem. Soc. (2014) 2–7.

[34] F. Klein, B. Jache, A. Bhide, P. Adelhelm, Phys. Chem. Chem. Phys. 15 (2013) 15876–15887.

[35] I. Hasa, R. Verrelli, J. Hassoun, Electrochim. Acta. 173 (2015) 613–618.

[36] A. Darwiche, C. Marino, M.T. Sougrati, B. Fraisse, L. Stievano, L. Monconduit, J. Am. Chem. Soc. 134 (2012) 20805–20811.

[37] M.K. Datta, R. Epur, P. Saha, K. Kadakia, S.K. Park, P.N. Kumta, J. Power Sources. 225 (2013) 316–322.

[38] C. Bommier, X. Ji, Recent Development on Anodes for Na-Ion Batteries, Isr. J. Chem. 55 (2015) 486–507.

[39] Y. Wen, K. He, Y. Zhu, F. Han, Y. Xu, I. Matsuda, et al., Nat. Commun. (2014).

[40] S. Komaba, T. Ishikawa, N. Yabuuchi, W. Murata, A. Ito, Y. Ohsawa, ACS Appl. Mater. Interfaces. 3 (2011) 4165–4168.

[41] H.Q. Pham, K.-M. Nam, E.-H. Hwang, Y.-G. Kwon, H.M. Jung, S.-W. Song, J. Electrochem. Soc. 161 (2014) A2002–A2011.

[42] A. Stokosa, J. Molenda, D. Than, Solid State Ionics. 15 (1985) 211–216.

[43] T. Shibata, Y. Fukuzumi, W. Kobayashi, Y. Moritomo, Sci. Rep. 5 (2015) 9006.

[44] H. Kim, J. Hong, Y.-U. Park, J. Kim, I. Hwang, K. Kang, Adv. Funct. Mater. 25 (2015) 534–541.

[45] Z. Yang, J. Zhang, M.C.W. Kintner-Meyer, X. Lu, D. Choi, J.P. Lemmon, et al., Chem. Rev. 111 (2011) 3577–3613.

Figure Captions

Figure 1. (a) X ray diffraction patterns (XRD) and **(b)** scanning electron microscopy images (SEM) of the $Na_{0.7}CoO_2$ material.

Figure 2. Galvanostatic responses at 0.2C rate in terms of voltage profile of the Na/1M $NaClO_4$ EC:DMC (1:1 w/w)/$Na_{0.7}CoO_2$ and **(b)** and Na/1M $NaClO_4$ EC:DMC (1:1 w/w) + 20% FEC/$Na_{0.7}CoO_2$ sodium half-cells. **(c)** Comparison of the cycling behavior in terms of stability and efficiency. 1C corresponds to 175 mA g^{-1}. Voltage range: 2.0-3.8 V vs Na^+/Na. Room temperature (20 ºC).

Figure 3 (a) Voltage profiles and **(b)** cycling behavior of the Na/1M $NaClO_4$ EC:DMC (1:1 w:w) + 20% FEC /$Na_{0.7}CoO_2$ cell studied at increasing currents. 1C corresponds to 175 mA g^{-1}. Voltage range: 2.0-3.8 V vs Na^+/Na. Room temperature (20 ºC).

Figure 4. (a) Voltage profiles of the galvanostatic cycling tests of a Na/Graphite half-cell employing the various electrolytes (see experimental section for details). **(b)** Long term cycling behavior at 1C rate of a Na/1M$NaClO_4$-TEGDME/Graphite half-cell and, in inset, corresponding voltage profile at the 1^{st}, 100^{th} and 500^{th} cycle. **(c)** Cycling performance of a Na/1M$NaClO_4$-TEGDME/Graphite half-cell at increasing current densities and **(d)** corresponding voltage profiles within 0.02-2.0 V vs Na^+/Na range, 1C = 200 mA g^{-1}. Room temperature (20 ºC).

Figure 5. (a) Voltage profiles at various cycle number of the Graphite/1M $NaClO_4$-TEGDME /$Na_{0.7}CoO_2$ full-cell galvanostatically cycled at 1C (175 mA g^{-1}) within the 0.5-3.7 V voltage range at room temperature (20 ºC). **(b)** Voltage profiles of the Graphite/1M $NaClO_4$-TEGDME /$Na_{0.7}CoO_2$ full cell galvanostatically cycled at various current rates and **(c)** and corresponding cycling responses within the 0.5-3.7 V voltage. **(d)** Prolonged galvanostatic cycling of a Graphite/1M $NaClO_4$-TEGDME /$Na_{0.7}CoO_2$ full-cell performed at 10C rate (1.75 A g^{-1}). 1C corresponds to 200 mA g^{-1}. Room temperature (20 ºC).

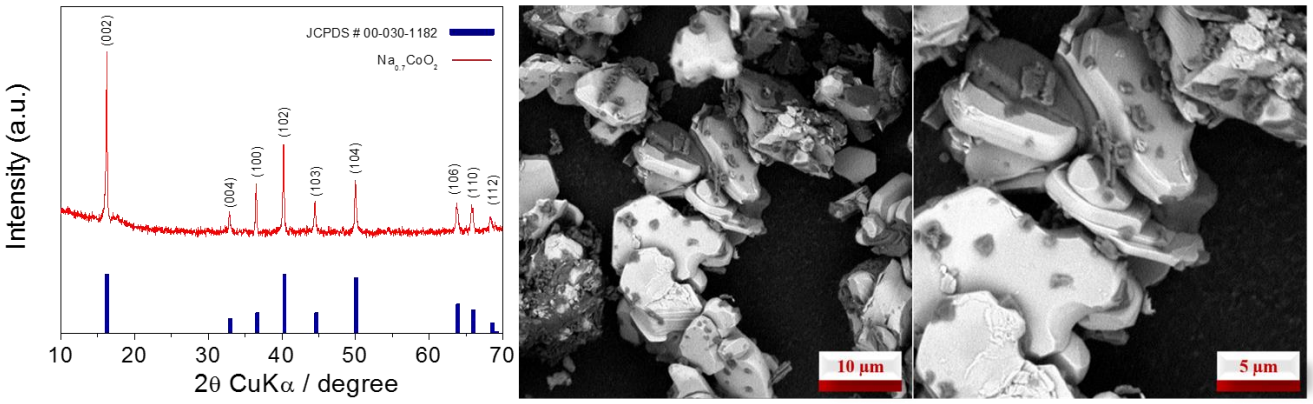
Intensity (a.u.)
JCPDS # 00-030-1182
Na0.7CoO2
(002)
(004)
(100)
(102)
(103)
(104)
(106)
(110)
(112)
10
20
30
40
50
60
70
2θ CuKα / degree
10 μm
5 μm

(a) (b)

Figure 1

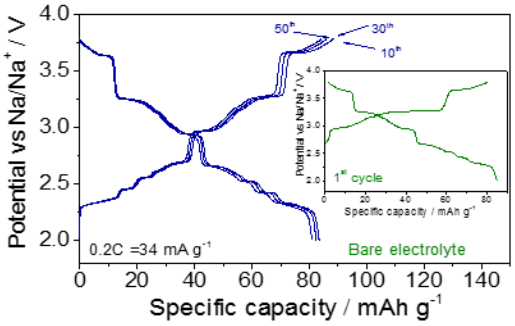
Potential vs Na/Na+ / V
Specific capacity / mAh g-1
50th
30th
10th
1st cycle
0.2C =34 mA g-1
Bare electrolyte

(a)

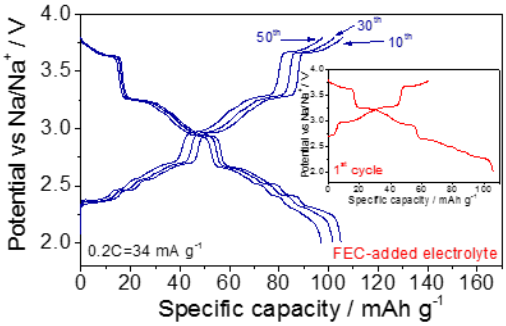
Potential vs Na/Na+ / V
Specific capacity / mAh g-1
50th
30th
10th
1st cycle
0.2C=34 mA g-1
FEC-added electrolyte

(b)

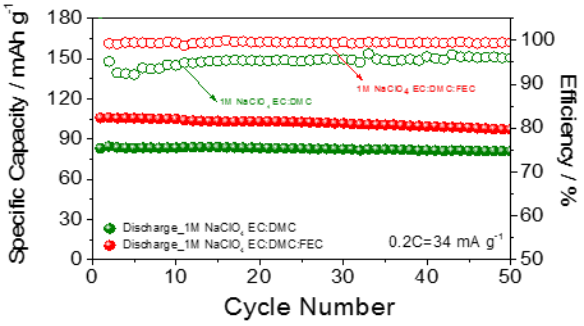
Specific Capacity / mAh g-1
Efficiency / %
Cycle Number
1M NaClO4 EC:DMC
1M NaClO4 EC:DMC:FEC
Discharge_1M NaClO4 EC:DMC
Discharge_1M NaClO4 EC:DMC:FEC
0.2C=34 mA g-1

(c)

Figure 2

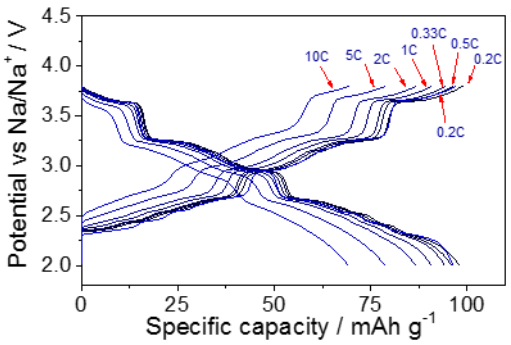
Potential vs Na/Na+ / V
Specific capacity / mAh g-1
10C
5C
2C
1C
0.33C
0.5C
0.2C
0.2C

(a)

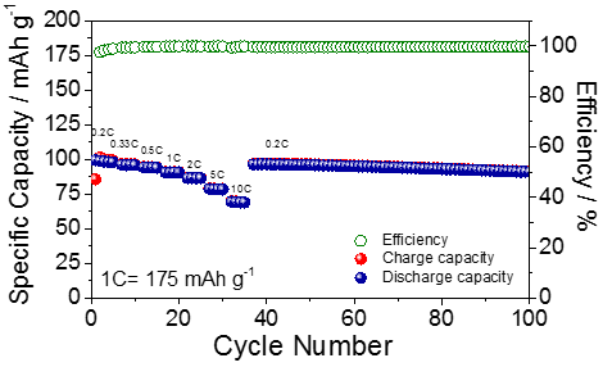
Specific Capacity / mAh g-1
Efficiency / %
Cycle Number
1C= 175 mAh g-1
Efficiency
Charge capacity
Discharge capacity
0.2C
0.33C
0.5C
1C
2C
5C
10C
0.2C

(b)

Figure 3

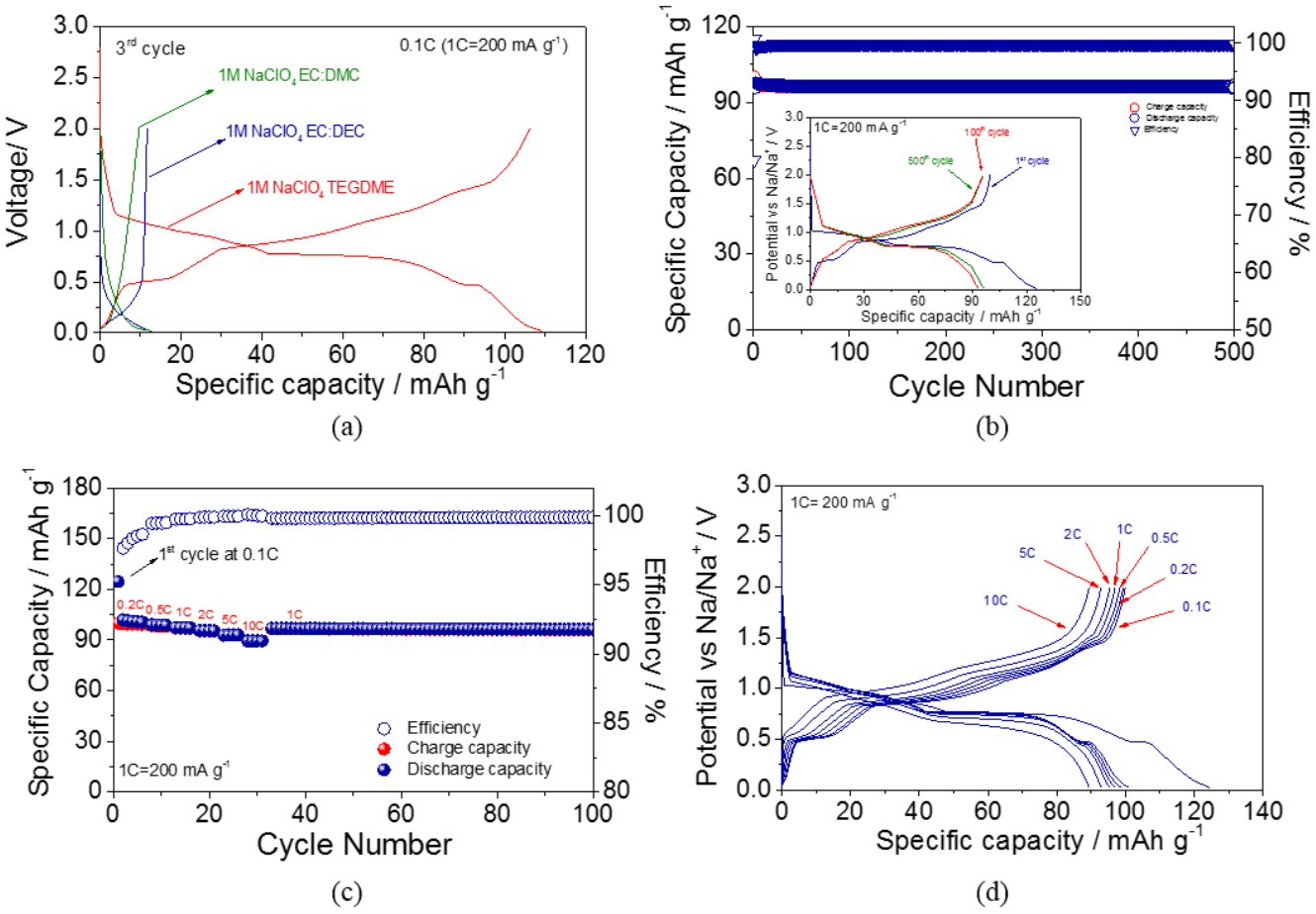
3rd cycle
0.1C (1C=200 mA g-1)
1M NaClO4 EC:DMC
1M NaClO4 EC:DEC
1M NaClO4 TEGDME
Voltage/ V
Specific capacity / mAh g-1
(a)
Specific Capacity / mAh g-1
Efficiency / %
Cycle Number
1C=200 mA g-1
100th cycle
500th cycle
1st cycle
Potential vs Na/Na+ / V
Specific capacity / mAh g-1
(b)
1st cycle at 0.1C
0.2C 0.5C 1C 2C 5C 10C 1C
Efficiency
Charge capacity
Discharge capacity
1C=200 mA g-1
Specific Capacity / mAh g-1
Efficiency / %
Cycle Number
(c)
1C= 200 mA g-1
5C
2C
1C
0.5C
0.2C
0.1C
10C
Potential vs Na/Na+ / V
Specific capacity / mAh g-1
(d)

Figure 4

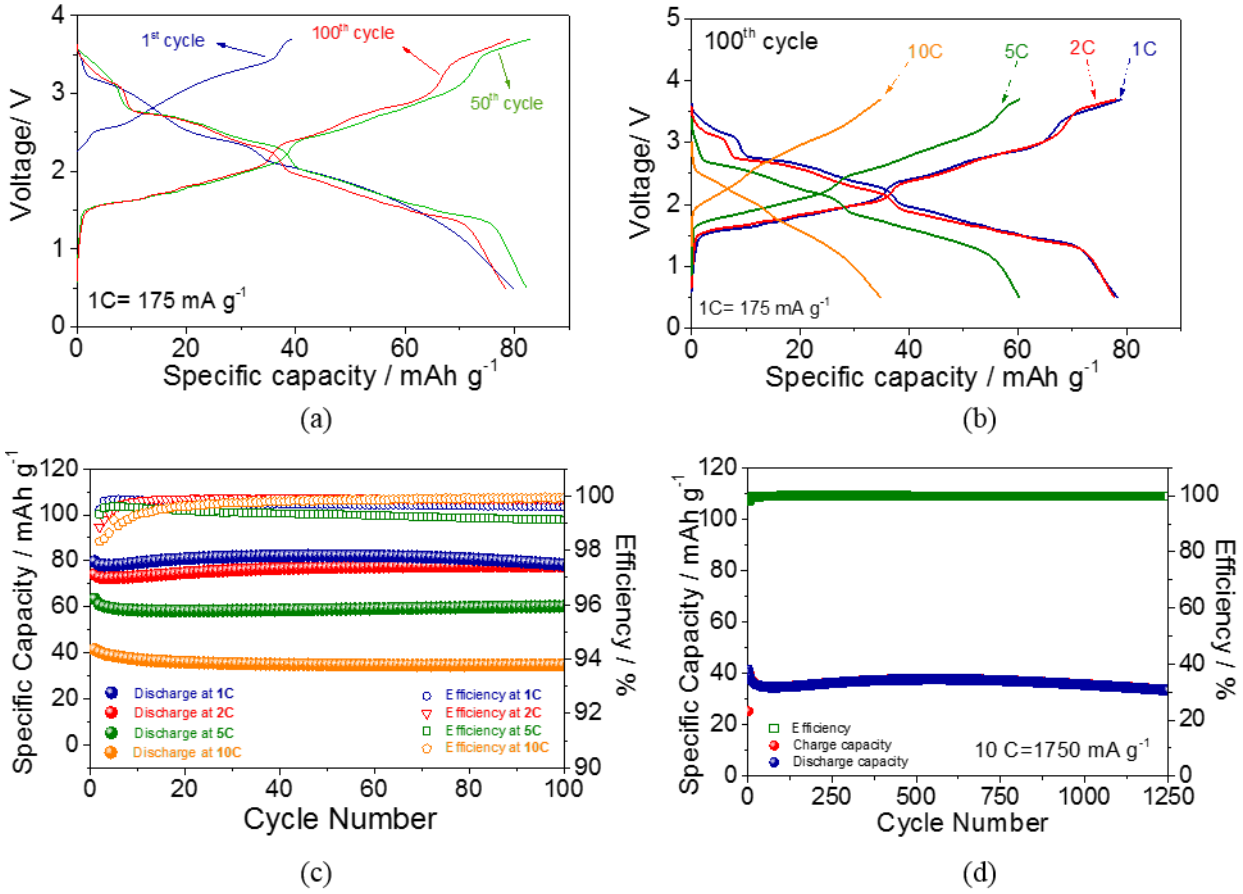
1st cycle
100th cycle
50th cycle
1C= 175 mA g-1
Voltage/ V
Specific capacity / mAh g-1
(a)
100th cycle
10C
5C
2C
1C
1C= 175 mA g-1
Voltage/ V
Specific capacity / mAh g-1
(b)
Specific Capacity / mAh g-1
Efficiency / %
Discharge at 1C
Discharge at 2C
Discharge at 5C
Discharge at 10C
Efficiency at 1C
Efficiency at 2C
Efficiency at 5C
Efficiency at 10C
Cycle Number
(c)
Specific Capacity / mAh g-1
Efficiency / %
Efficiency
Charge capacity
Discharge capacity
10 C=1750 mA g-1
Cycle Number
(d)

Figure 5